

# Convective heat transport in stratified atmospheres at low and high Mach number

Evan H. Anders and Benjamin P. Brown

*Department of Astrophysical & Planetary Sciences, University of Colorado – Boulder and  
Laboratory for Atmospheric and Space Physics, Boulder, CO*

Here we study stratified convection in the context of plane-parallel, polytropically stratified atmospheres. We hold the density stratification ( $n_\rho$ ) and Prandtl number (Pr) constant while varying the Mach number (Ma) and the Rayleigh number (Ra) to determine the behavior of the Nusselt number (Nu), which quantifies the efficiency of convective heat transport. As Ra increases and  $Ma \rightarrow 1$ , a scaling of  $Nu \propto Ra^{0.45}$  is observed. As Ra increases to a regime where  $Ma \geq 1$ , this scaling gives way to a weaker  $Nu \propto Ra^{0.19}$ . In the regime of  $Ma \ll 1$ , a consistent  $Nu \propto Ra^{0.31}$  is retrieved, reminiscent of the  $Nu \propto Ra^{2/7}$  seen in Rayleigh-Bénard convection.

## INTRODUCTION

Convection is essential to heat transport in the cores of high mass stars, the envelopes of low mass stars, and the atmospheres of terrestrial and jovian planets. The convective dynamics are influenced by the atmospheric stratification, which is small in some systems but extends up to 14 density scale heights in the Sun’s convective envelope. Understanding the fundamental properties of compressible convection in stratified media is essential to characterizing systems in astrophysics and planetary sciences. Numerical constraints have often restricted studies of compressible convection to moderately high Mach number (Ma), appropriate to regions near the Sun’s surface. Few fundamental properties of the low-Ma stratified convection which occurs in the deep solar interior are known.

Early numerical experiments on stratified convection in two [1–4] and three [5, 6] dimensions revealed a number of basic properties in the moderate-to-high Ma regime. In the widely-studied Rayleigh-Bénard (hereafter RB) problem, upflows and downflows are symmetrical and the temperature gradient approaches zero in the convective interior causing the conductive flux to similarly disappear. Highly stratified convection exhibits narrow downflow lanes and broad upflow regions. Furthermore, the entropy gradient is negated by convection rather than the temperature gradient, such that in the presence of perfectly efficient convection a significant component of the flux is still carried by conduction.

In RB convection, there exist two primary control parameters: the Rayleigh number (Ra, the ratio of buoyant driving to diffusive damping) and the Prandtl number (Pr, the ratio of viscous to thermal diffusivity). These numbers coupled with the aspect ratio of the physical domain and the boundary conditions determine the dynamics of the convection. In stratified atmospheres, in addition to specifying the equation of state and fundamental properties of the gas, the two control parameters of RB convection are joined by the degree of stratification across the domain and the characteristic Ma of the convective flows. Polytropically stratified atmospheres,

such as those used in early studies, are an ideal extension of RB convection into the stratified realm as the two additional control parameters are directly linked to basic properties of the atmosphere. The density stratification is set by the number of density scale heights the atmosphere spans ( $n_\rho$ ), and Ma is controlled by the superadiabatic excess ( $\epsilon$ , the deviation of the polytropic index from the adiabatic polytropic index [1]).

In this letter we study the behavior of convective heat transport, quantified by the Nusselt number (Nu), in plane-parallel, two-dimensional, polytropically stratified atmospheres.  $\epsilon$  and Ra are varied while  $n_\rho$ , Pr, and the aspect ratio are held constant. In section II, the construction of atmospheres, equations, and numerical methods are discussed. Results are described in section III and their implications are discussed in section IV.

## EXPERIMENT

In order to compare our results with previous studies and in an effort to examine a simplest case, we study a fluid composed of monatomic ideal gas particles with an adiabatic index of  $\gamma = 5/3$  and whose equation of state is  $P = R\rho T$ . The initial atmosphere is a plane-parallel polytrope in which the gravitational acceleration and conductive flux,  $\mathbf{F}_{\text{cond},0} = -\kappa\nabla T_0$ , do not vary with depth. To achieve the latter condition, both  $\kappa$  and  $\nabla T_0$  are constant. Under these assumptions, satisfying hydrostatic equilibrium produces a stratification of

$$\begin{aligned}\rho_0(z) &= \rho_t(z_0 - z)^m, \\ T_0(z) &= T_t(z_0 - z),\end{aligned}\tag{1}$$

where  $m = m_{ad} - \epsilon$  is the polytropic index. The adiabatic polytropic index is  $m_{ad} \equiv (\gamma - 1)^{-1}$  and the superadiabatic excess is  $\epsilon$  which sets the scale of the entropy gradient,  $\nabla S_0 \propto -\epsilon$ . Thermodynamic variables are nondimensionalized at the top of the atmosphere as  $P_0(L_z) = \rho_0(L_z) = T_0(L_z) = 1$ , requiring  $z_0 \equiv L_z + 1$  and  $R = T_t = \rho_t = 1$ . By this choice, the non-dimensional length scale is the inverse temperature gradient scale and the timescale is the isothermal sound crossing time

of this unit length.  $z$  increases upwards within  $[0, L_z]$ , where  $L_z = e^{n_\rho/m} - 1$  is determined by  $n_\rho$ , the number of density scale heights the atmosphere spans. The characteristic timescale of convective dynamics is related to the atmospheric buoyancy time,  $t_b = \sqrt{L_z/g\epsilon}$ , with  $g = (m+1)$ . Throughout this letter, buoyancy time units are used and  $n_\rho = 3$  such that the initial density varies by a factor of 20. All atmospheres studied here have an aspect ratio of 4, such that  $L_x = 4L_z$ .

Atmospheric diffusivities are specified by the Rayleigh number and the Prandtl number. The non-dimensional Rayleigh number is

$$\text{Ra} = \frac{gL_z^3(\Delta S_0/c_P)}{\nu\chi}, \quad (2)$$

where  $\Delta S_0$  is the entropy difference between the top and bottom of the atmosphere,  $c_P = R\gamma(\gamma-1)^{-1}$  is the specific heat at constant pressure,  $\nu$  is the kinematic viscosity (viscous diffusivity), and  $\chi$  is the thermal diffusivity. The relationship between the thermal and viscous diffusivities is set by the Prandtl number,  $\text{Pr} = \nu/\chi$ . We relate the dynamic viscosity,  $\mu$ , and the thermal conductivity,  $\kappa$ , to their corresponding diffusivities such that  $\nu \equiv \mu/\rho$  and  $\chi \equiv \kappa/\rho$ . As a result,  $\text{Ra} \propto (\nu\chi)^{-1} \propto \rho^2$ . The atmospheres studied here with  $n_\rho = 3$  experience an increase in the Rayleigh number by a factor of 400 across the domain. This formulation leaves  $\text{Pr}$  constant throughout the depth of the atmosphere. In this letter we impose  $\text{Pr} = 1$  and specify  $\text{Ra}$  at  $z = L_z$ .

At the constant values of  $n_\rho$  and  $\text{Pr}$  used, the primary control parameters of convection are  $\epsilon$  and  $\text{Ra}$ . We decompose our atmosphere into the background polytrope ( $\ln \rho_0, T_0$ ) and the fluctuations about that background ( $\mathbf{u}, \ln \rho_1, T_1$ ). The scaling of the entropy gradient with  $\epsilon$  is reflected in the evolved values of these fluctuations, which follow the scaling of  $T_1/T_0 \propto \rho_1/\rho_0 \propto \text{Ma}^2 \propto \epsilon$  for low values of  $\epsilon$ , as in Fig. 1.

The Fully Compressible Navier-Stokes equations,

$$\frac{\partial \ln \rho}{\partial t} + \nabla \cdot (\mathbf{u}) = -\mathbf{u} \cdot \nabla \rho, \quad (3)$$

$$\begin{aligned} \frac{\partial \mathbf{u}}{\partial t} + \nabla T - \nu \nabla \cdot (\bar{\sigma}) - \bar{\sigma} \cdot \nabla \nu = \\ -\mathbf{u} \cdot \nabla \mathbf{u} - T \nabla \ln \rho + \mathbf{g} + \nu \bar{\sigma} \cdot \nabla \ln \rho, \end{aligned} \quad (4)$$

$$\begin{aligned} \frac{\partial T}{\partial t} - \frac{1}{c_V} (\chi \nabla^2 T + \nabla T \cdot \nabla \chi) = \\ -\mathbf{u} \cdot \nabla T - (\gamma - 1) T \nabla \cdot (\mathbf{u}) \\ + \frac{1}{c_V} (\chi \nabla T \cdot \nabla \ln \rho + \nu [\bar{\sigma} \cdot \nabla] \cdot \mathbf{u}), \end{aligned} \quad (5)$$

are evolved with a viscous stress tensor defined as

$$\sigma_{ij} \equiv \left( \frac{\partial u_i}{\partial x_j} + \frac{\partial u_j}{\partial x_i} - \frac{2}{3} \delta_{ij} \nabla \cdot (\mathbf{u}) \right). \quad (6)$$

Taking an inner product of Eq. 4 with  $\mathbf{u}$  and adding

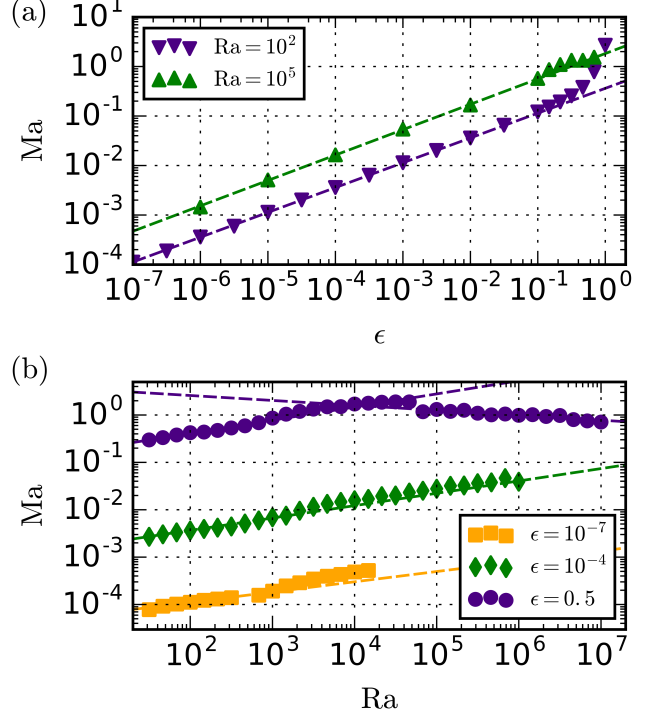


FIG. 1. The maximum value of Ma which has been horizontally averaged and time averaged for  $\geq 100t_b$ , beginning roughly  $50t_b$  after the start of simulations. This time average is long enough that the profile is well converged and error bars are negligible. (a) For  $\epsilon \leq 0.1$ , a scaling of  $\text{Ma} \propto \{\epsilon^{0.50}, \epsilon^{0.51}\}$  at  $\text{Ra} = \{10^2, 10^5\}$  exists. When  $\epsilon \rightarrow m_{ad}$ , large deviations from this power law are seen. (b) At high  $\epsilon$ , Ma scales as  $\text{Ra}^{0.28}$  until it reaches the supersonic regime, at which point it follows a power law of  $\text{Ra}^{-0.10}$ . At low  $\epsilon$ , consistent power laws are achieved throughout all values of Ra studied, where  $\text{Ma} \propto \{\text{Ra}^{0.26}, \text{Ra}^{0.22}\}$  for  $\epsilon = \{10^{-4}, 10^{-7}\}$ .

it to Eq. 5 reveals the full energy equation,

$$\frac{\partial}{\partial t} \left( \rho \left[ \frac{|\mathbf{u}|^2}{2} + c_V T + \phi \right] \right) + \nabla \cdot (\mathbf{F}_{\text{conv}} + \mathbf{F}_{\text{cond}}) = 0. \quad (7)$$

The convective flux is  $\mathbf{F}_{\text{conv}} \equiv \mathbf{F}_{\text{enth}} + \mathbf{F}_{\text{KE}} + \mathbf{F}_{\text{PE}} + \mathbf{F}_{\text{visc}}$ . Contributions from the enthalpy flux,  $\mathbf{F}_{\text{enth}} \equiv \rho \mathbf{u} (c_V T + P/\rho)$ ; the kinetic energy flux,  $\mathbf{F}_{\text{KE}} \equiv \rho |\mathbf{u}|^2 \mathbf{u}/2$ ; the potential energy flux,  $\mathbf{F}_{\text{PE}} \equiv \rho \mathbf{u} \phi$  (with  $\phi \equiv -gz$ ); and the viscous flux,  $\mathbf{F}_{\text{visc}} \equiv -\rho \nu \mathbf{u} \cdot \bar{\sigma}$ , must all be considered. Understanding these flux terms and how they interact with the conductive flux,  $\mathbf{F}_{\text{cond}} = -\kappa \nabla T$ , is crucial in characterizing convective heat transport.

The atmosphere is contained between two impenetrable, stress free, fixed temperature boundaries at the top and bottom of the domain such that  $w = \partial_z u = T_1 = 0$  at  $z = \{0, L_z\}$ . The domain is horizontally periodic. We utilize the novel Dedalus<sup>1</sup> pseudospectral frame-

<sup>1</sup> <http://dedalus-project.org/>

work to time-evolve Eqs. 3-5 using an implicit-explicit, third-order, four-step Runge-Kutta timestepping scheme RK443 [7]. Variables are time-evolved on a dealiased Chebyshev (vertical) and Fourier (horizontal) domain in which the physical grid dimensions are 3/2 the size of the coefficient grid. Physical grid sizes range from 96x384 grid points at the lowest values of Ra to 1152x4608 grid points at  $\text{Ra} \geq 10^7$ . By using IMEX timestepping, we implicitly step the stiff linear acoustic wave contribution and are able to efficiently study flows at moderate ( $\approx 1$ ) and very low ( $\approx 10^{-4}$ ) Ma (Fig. 1b). Our equations take the form of the FC equations in [8], extended to include variable  $\nu$  and  $\chi$ , and we follow the approach there; this IMEX approach has been successfully tested against a nonlinear benchmark of the compressible Kelvin-Helmholtz instability [9].

## RESULTS

The efficiency of convection is quantified by the Nusselt number. Nu is well-defined in RB convection as the total flux normalized by the steady-state conductive flux [10, 11]. In stratified convection Nu is more difficult to define, but one of the earliest definitions used was [1, 3]

$$\text{Nu} \equiv \frac{F_{\text{conv}, z} + F_{\text{cond}, z} - F_A}{F_{\text{ref}} - F_A}, \quad (8)$$

where  $F_{\text{conv}, z}$  and  $F_{\text{cond}, z}$  are the z-components of  $\mathbf{F}_{\text{conv}}$  and  $\mathbf{F}_{\text{cond}}$ , respectively.  $F_A \equiv -\kappa \partial_z T_{\text{ad}}$  is the adiabatic conductive flux and  $\partial_z T_{\text{ad}} \equiv -g/c_P$  for an ideal gas in hydrostatic equilibrium.  $F_{\text{ref}} \equiv \Delta T/L_z$ , where  $\Delta T \equiv T(L_z) - T(0)$ , is the conductive flux of a linear profile connecting the upper and lower plates, which is constant for the choice of fixed-temperature boundaries.

We contend that this is the general form of the Nusselt number and illustrate this with a few limiting cases. Convection eliminates entropy stratification. Under the Boussinesq approximation, in which density variations are ignored, entropy stratification is directly proportional to temperature stratification such that  $\nabla S \rightarrow 0$  when  $\nabla T \rightarrow 0$ . The familiar Nu in the RB problem is therefore retrieved from Eq. 8 because  $\nabla T_{\text{ad}} = 0$ . In the case of polytropic convection,  $g \rightarrow 0$  as  $\epsilon \rightarrow m_{\text{ad}} + 1$ . In this limit,  $F_A \rightarrow 0$  and the definition of the RB Nu is appropriate to use, as convection carries all of the flux [12]. However, as  $\epsilon \rightarrow 0$ ,  $\nabla T_{\text{ad}} \rightarrow \nabla T_0$  and increasingly smaller velocity and thermodynamic perturbations are needed to achieve  $\nabla S = 0$  (Fig. 1a). These perturbations carry what little flux exists in excess of the adiabatic, so the removal of  $F_A$  in the numerator and denominator of Eq. 8 is essential for a reasonable Nu measurement.

Initial value problems were solved in which  $T_1$  was filled with infinitesimal, random noise compared to  $T_0$  and  $\epsilon$ . Solutions were time-evolved until a long average of Nu showed little variance with depth. By performing

a linear stability analysis, we determined that the onset of convection occurs at  $\text{Ra}_c = \{10.06, 10.97, 10.97\}$  for  $\epsilon = \{0.5, 10^{-4}, 10^{-7}\}$ , respectively. We studied Rayleigh numbers from values at onset up to nearly  $10^6 \text{Ra}_c$  for  $\epsilon = 0.5$ ,  $10^5 \text{Ra}_c$  for  $\epsilon = 10^{-4}$ , and  $10^3 \text{Ra}_c$  for  $\epsilon = 10^{-7}$ .

At large Ma ( $\epsilon = 0.5$ ), shock systems form in the upper atmosphere near downflow lanes (Fig. 2a) and propagate toward upflow lanes. Such systems were reported in both two [4] and three [13] dimensional polytropic simulations previously. These shocks heat material entering the downflows, affecting the dynamics and heat transport of these systems.

Low Ma flows ( $\epsilon = 10^{-4}$ ) have similar bulk thermodynamic structures (Fig. 2b). As Ra is increased to large values (Fig. 2c), thermodynamic structures no longer span the whole domain but rather break up into small packets which traverse the domain multiple times before diffusing. While it has been suggested that pressure forces cause symmetry breaking in up- and downflows, [3], this effect seems to be secondary to flows obeying mass conservation as they traverse the stratified medium. We observe low Ma cases where the double-roll systems such as those in Fig. 2b contain one roll of increased

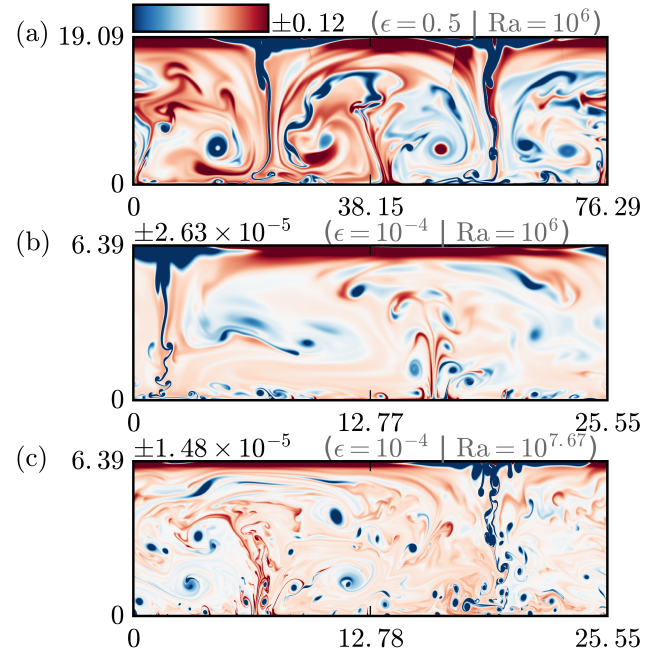


FIG. 2. Characteristic entropy fluctuations in evolved flows. The time- and horizontally- averaged profile is removed in all cases. At high  $\epsilon$  (a), shock systems form near the upper downflow lanes and propel shock-heated material deep within the atmosphere at sufficiently high Ra. At low  $\epsilon$  but at the same Ra (b), shock systems are absent, but otherwise the dynamics are similar. As Ra is increased (c), downflow lanes no longer span the entirety of the domain and individual small blobs are responsible for carrying the flux.

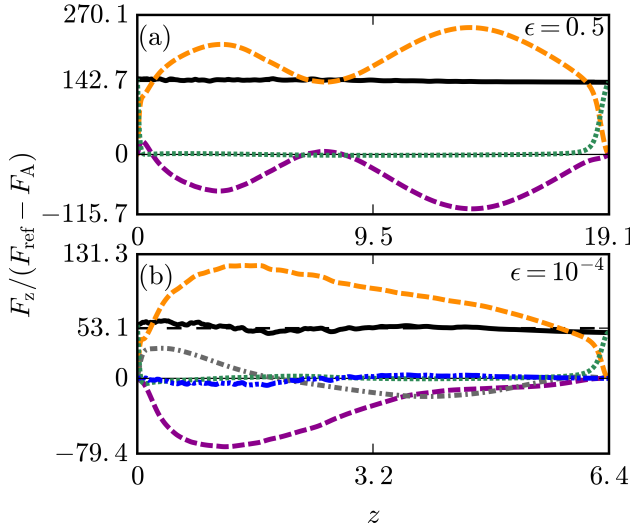


FIG. 3. Time-averaged flux profiles for high (a) and low (b) Ma flows at  $\text{Ra} = 10^6$ . The dashed lines correspond to the enthalpy flux (orange, positive) and kinetic energy flux (purple, negative). The grey dash-dot line is the viscous flux, the blue dash-dot-dot line is the potential energy flux, and the green dotted line is the radiative flux with the adiabatic radiative flux removed. Viscous and potential energy fluxes are negligible in (a) and are not shown. All fluxes are normalized by  $F_{\text{ref}} - F_A$ , as in Eq. 8. The solid black line is Nu, the properly normalized sum of all the fluxes

pressure and one roll of decreased pressure where the up- and downflows bound these regions of pressure disequilibrium.

at large values of Ra in which shocks form, high Ma flows exhibit two local maxima in the enthalpy flux and kinetic energy flux (Fig. 3a). Shock-heated fluid parcels sometimes spin-up as they are pushed into the lower atmosphere, creating deep, rapidly-rotating regions of mixing which persist for many overturn times. These “spinners” sit inside of larger rolls created by their neighboring up- and downflows and greatly influence the dynamics. At low Ma, only the deep maximum is present (Fig. 3b). Fixed-temperature boundary conditions allow the flux at the boundaries to vary, so many runs at  $\text{Ra} > 10^5$  and  $\epsilon = 10^{-4}$  exhibit states in which the flux entering the system at the bottom of the atmosphere exceeds that which leaves at the top. These states are punctuated by states of vigorous shearing, similar to those previously reported in two-dimensional RB convection [14]. These shearing states push the bottom temperature gradient towards adiabatic, allowing the excess energy to exit through the upper boundary. These shearing states will be covered in more detail in a future paper. Regardless, a proper long-term average over shearing and non-shearing states retrieves an invariant flux (and Nu) profile throughout the depth of the atmosphere.

After appropriately time-averaging the fluxes for  $\geq$

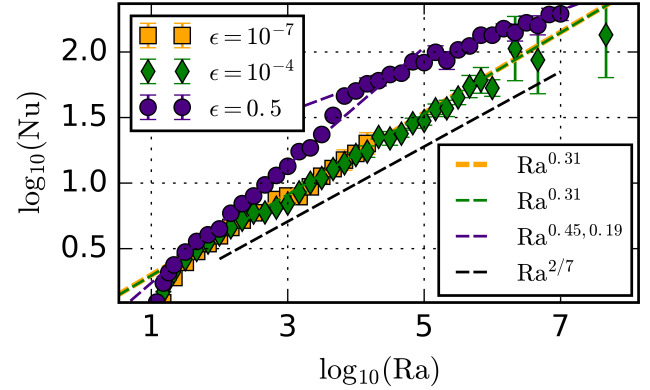


FIG. 4. Variation of Nu as Ra increases at low and high Ma. At high  $\epsilon$  (purple circles), a clear transition from the subsonic to supersonic regime is evident in the scaling of Nu with Ra. In the low  $\epsilon$  regime (green diamonds and yellow squares), Nu scalings collapse onto a similar line which is **consistent with RB scalings?** [10]. Error bars are determined by the square root of the variance of Nu with depth and indicate whether or not a solution is well-converged.

$200t_b$ , a sensible Nu is retrieved. Nusselt numbers for all simulations at low and high Ma are plotted in Fig. 4. At  $\epsilon = \{10^{-4}, 10^{-7}\}$ , scaling laws of  $\text{Nu} \propto \text{Ra}^{\{0.31, 0.31\}}$  are retrieved. At  $\epsilon = 0.5$ , in the near-sonic regime ( $\text{Ra} \leq 10^4$ ), the scaling of Nu with Ra is inflated, with  $\text{Nu} \propto \text{Ra}^{0.45}$ . As simulations pass into the supersonic regime and shocks start to form near the downflows, that scaling drops to  $\text{Nu} \propto \text{Ra}^{0.19}$ .

## DISCUSSION

In this letter we have studied fundamental heat transport by stratified convection in simplified 2-D polytropic atmospheres which are specified by two parameters,  $n_\rho$  and  $\epsilon$ . We argue that these atmospheres are the natural extension of the RB problem to stratified systems, and should be used to understand the basic properties of stratified convection. The similarity between the scaling of Nu in RB convection and in low- $\epsilon$  polytropes suggests that a boundary layer theory such as the Grossmann-Lohse theory for incompressible flows could be developed for fully compressible convection in these systems [15].

The dynamics of these polytropic solutions are complex and highly time-dependent, even in two dimensions. Time-dependent oscillating shear states have developed spontaneously, as seen before in RB convection [14]. While computationally difficult, the highest values of Ra and the lowest value of  $\epsilon$  studied here are far from values found in nature. If the scalings of Nu and Ma presented here (Figs. 1 & 4) hold, then under solar conditions ( $\text{Ra} \approx 10^{20}$ ,  $\text{Ma} \approx 10^{-4}$ ), we expect that  $\epsilon \approx 10^{-20}$  and  $\text{Nu} \approx 10^6$ . Solar conditions are of course more compli-

cated, as there  $\kappa$  is set by the radiative opacity, which depends on both  $\rho$  and  $T$ .

Future work will aim to better understand the mechanisms of shearing states and whether or not these states are attainable in three-dimensional, non-rotating atmospheres. Our studies here have set the groundwork for understanding and comparing heat transport in stratified convection to that in RB convection [10], and for future studies of transport in stratified convection in more realistic systems, such as those bounded by stable regions [16] or using more realistic profiles of  $\kappa$ .

### acknowledgements

EHA acknowledges the support of the University of Colorado's George Ellery Hale Graduate Student Fellowship. This work was supported by NASA LWS grant number NNX16AC92G. Computations were conducted with support by the NASA High End Computing (HEC) Program through the NASA Advanced Supercomputing (NAS) Division at Ames Research Center with allocations (GID s1647, PI Brown; GID g26133, PI Toomre). We thank Axel Brandenburg, Mark Rast, and Jeff Oishi for many useful discussions.

- 
- [2] K. L. Chan, S. Sofia, and C. L. Wolff, *Astrophys. J.* **263**, 935 (1982).
  - [3] N. E. Hurlburt, J. Toomre, and J. M. Massaguer, *Astrophys. J.* **282**, 557 (1984).
  - [4] F. Cattaneo, N. E. Hurlburt, and J. Toomre, *ApJL* **349**, L63 (1990).
  - [5] F. Cattaneo, N. H. Brummell, J. Toomre, A. Malagoli, and N. E. Hurlburt, *Astrophys. J.* **370**, 282 (1991).
  - [6] N. H. Brummell, N. E. Hurlburt, and J. Toomre, *Astrophys. J.* **473**, 494 (1996).
  - [7] U. M. Ascher, S. J. Ruuth, and R. J. Spiteri, *Applied Numerical Mathematics* **25**, 151 (1997).
  - [8] D. Lecoanet, B. P. Brown, E. G. Zweibel, K. J. Burns, J. S. Oishi, and G. M. Vasil, *Ap. J.* **797**, 94 (2014), 1410.5424.
  - [9] D. Lecoanet, M. McCourt, E. Quataert, K. J. Burns, G. M. Vasil, J. S. Oishi, B. P. Brown, J. M. Stone, and R. M. O'Leary, *MNRAS* **455**, 4274 (2016), 1509.03630.
  - [10] H. Johnston and C. R. Doering, *Physical Review Letters* **102**, 064501 (2009), 0811.0401.
  - [11] J. Otero, R. W. Wittenberg, R. A. Worthing, and C. R. Doering, *Journal of Fluid Mechanics* **473**, 191 (2002).
  - [12] A. Brandenburg, K. L. Chan, Å. Nordlund, and R. F. Stein, *Astronomische Nachrichten* **326**, 681 (2005), astro-ph/0508404.
  - [13] A. Malagoli, F. Cattaneo, and N. H. Brummell, *ApJL* **361**, L33 (1990).
  - [14] D. Goluskin, H. Johnston, G. R. Flierl, and E. A. Spiegel, *Journal of Fluid Mechanics* **759**, 360 (2014).
  - [15] G. Ahlers, S. Grossmann, and D. Lohse, *Rev. Mod. Phys.* **81**, 503 (2009).
  - [16] N. E. Hurlburt, J. Toomre, and J. M. Massaguer, *Astrophys. J.* **311**, 563 (1986).

[1] E. Graham, *Journal of Fluid Mechanics* **70**, 689 (1975).